Ethylene and 1-Hexene Sorption in LLDPE under Typical Gas Phase Reactor Conditions: A Priori Simulation and Modeling for Prediction of Experimental Observations

Brian J. Banaszak,[†] Dennis Lo,[‡] Tomy Widya,[§] W. Harmon Ray,[⊥] and Juan J. de Pablo*

Department of Chemical and Biological Engineering, University of Wisconsin−Madison, Madison, Wisconsin 53706

Antonin Novak[||] and Juraj Kosek[#]

Department of Chemical Engineering, Prague Institute of Chemical Technology, Prague 16628, Czech Republic

Received May 6, 2004; Revised Manuscript Received August 28, 2004

ABSTRACT: A detailed study has been conducted of the sorption of ethylene and 1-hexene in linear low density polyethylene (LLDPE) under typical gas phase LLDPE reactor conditions. The recently proposed osmotic ensemble hyperparallel tempering method is used to simulate ethylene and 1-hexene gas sorption in the polymer samples. Simulations are used to parametrize the PC−SAFT equation of state for calculation of gas sorption in amorphous polyethylene. A model for crystallite induced elastic constraints is adopted to modify the equation of state for description of gas sorption in polyethylene below melting point conditions. Single-component ethylene and 1-hexene gas sorption as well as ethylene/1-hexene gas co-sorption are studied in this work. It is observed that simulations provide an effective method to parametrize the PC−SAFT equation of state. In addition, since simulations and PC−SAFT assume a hypothetically amorphous polymer, a quantitative description of elastic effects for gas sorption in semicrystalline polyethylene emerges from our approach. The results are verified by comparison to the experimental results of Novak et al. [Novak et al. Manuscript in preparation, 2004].

1. Introduction

In the commercial gas-phase manufacturing of linear low-density polyethylene (LLDPE), a higher α-olefin, typically 1-butene, 1-hexene, or 1-octene, is used as a comonomer. To develop a sound understanding of the kinetics of the polymerization process and, hence, the quality of the product resin, precise knowledge of the solubility and density of monomers or other small molecule solutes in polyethylene (PE) is required under reaction conditions.

The objective of this research is to use molecular simulations and a recently developed osmotic-ensemble hyper-parallel tempering technique[1] to arrive at an equation of state capable of predicting the solubility of monomers in LLDPE under typical reaction conditions. To reach this goal, results of simulations are used to fit and test the perturbed-chain statistical associating fluid theory (PC−SAFT) equation of state.[2−4] The PC−SAFT equation of state is a modification to the original SAFT[5−8] equation of state and has been shown to yield predictions that agree with measurements of solubility of small molecules in polyolefins when binary interaction parameters are fitted to experimental data.

[†] Current address: BASF AG, GKE, 67056 Ludwigshafen, Germany. E-mail: brian.banaszak@basf-ag.de.
[‡] Current address: DuPont Surfaces R&D, Buffalo, NY 14207. E-mail: Dennis.P.Lo@usa.dupont.com.
[§] Current address: Department of Chemical Engineering and Materials Science, University of Minnesota, Minneapolis, MN 55455. E-mail: twidya@cems.umn.edu.
[⊥] E-mail: ray@engr.wisc.edu.
* To whom correspondence should be addressed. E-mail: depablo@engr.wisc.edu.
[||] E-mail: Antonin.Novak@vscht.cz.
[#] E-mail: Juraj.Kosek@vscht.cz.

Under typical reaction conditions, LLDPE exists in a semicrystalline state. Our molecular simulations do not capture this semicrystalline structure because the level of detail required to capture crystallinity is not included in the united-atom force-field employed in this work and the length scale of this semicrystalline structure is much larger than the scale of our molecular simulations (our molecular simulations are conducted in periodic simulation cells of up to 40 Å in length and single crystallites in semicrystalline polyethylene are on the order of 100 Å in length). In addition, the PC−SAFT equation of state does not account for the effects of crystallites on the solubility of molecules in the amorphous portion of the semicrystalline structure. However, it has been proposed that with the introduction of crystallites, the swelling in the amorphous phase of the semicrystalline polymer is constrained, thereby reducing the solubility of molecules in the amorphous phase of the polymer as compared to that in a hypothetical, purely amorphous polymer under the same conditions. To account for this elastic constraint, following Michaels et al.,[9] we have adopted a simple modification of the PC−SAFT equation of state that permits calculation of thermodynamic properties. Such an approach has been reported to yield solubility predictions for aromatics in polyethylene[10] in good agreement with experiment. Further theoretical and experimental investigations of "constrained interphases" can be found in the literature.[11−14]

One point of particular interest in the study of monomer sorption in polymers is that of providing an understanding of the so-called "comonomer effect". The "comonomer effect" is the terminology used to explain observed increases in the ethylene polymerization rate due to the addition of a comonomer.[15−19] Under LLDPE

10.1021/ma0491107 CCC: $27.50
Published on Web 11/05/2004

reactor conditions, both ethylene and the higher α-olefin are present in the gas phase, and therefore, a fundamental understanding of this effect would have important practical value. Depending on the operating conditions of the reactor, the addition of 1-hexene has been observed either to cause no effect on the polymerization rate or to cause up to a 4-fold increase in the polymerization rate.[16,18] This so-called comonomer effect could have several origins. Recent evidence suggests that, in reaction mixtures of small molecule solutes (methane, ethylene, 1-hexene, and nitrogen) and linear amorphous PE, the solutes exhibit a tendency to aggregate near chain ends.[1,20,21] Short-chain branching in poly(ethylene-*co*-1-hexene), arising from varying amounts of 1-hexene in the reacting mixture, could lead to aggregation effects near branch chain ends. Previous work from our group[1] indicates that the aggregation effect induced by short-chain branching is counteracted by the increased density due to branching, leading to a monomer solubility which is essentially identical to that observed in a purely linear material. It is unclear, however, to what extent this observation prevails in the presence of a comonomer. It is known that, upon addition of 1-hexene to the gas phase, the solubility of ethylene increases (with respect to that for pure ethylene) as a result of the enhanced swelling of the polymer by the more soluble cosolvent (1-hexene).[21] Further discussions in light of the results presented here are provided below.

To test the predictive capabilities of our techniques, we have compared our predictions with the experimental results of Novak et al.[22] Novak et al. have measured the solubility of ethylene and 1-hexene in controlled ethylene-1-hexene copolymer samples prepared with a titanium-based Ziegler−Natta type catalyst in a gas-phase reactor. The ethylene to 1-hexene ratios incorporated in the LLDPE have been characterized and are similar to the polymer architectures that we have studied. Novak et al.[22] measured the monomer solubilities at conditions above and below the polymer melting temperature, thus providing data showing the effect of crystallites on the sorption of monomers in the amorphous polymer phase. Solubilities below the melting temperature were measured in nascent polymer powder. These samples are therefore representative of the polymer during reactor conditions.

2. Simulation Techniques

2.1. Force Field. All simulations employ the NERD force field,[20,23−25] in which united-atom sites represent CH_n groups in ethylene, 1-hexene, and polyethylene chain molecules. The bonded and nonbonded NERD force field parameters adopted in this work for ethylene, 1-hexene, and polyethylene chain molecules are provided in Table 1. A 12−6 Lennard-Jones potential energy function is adopted for nonbonded interactions. This includes site−site interactions for sites on the same molecule located more than three bonds apart and sites located on different molecules. For polyethylene chains and 1-hexene, a torsional potential energy function is imposed on rotations about carbon−carbon bonds.[26] Bond stretching and bond-angle bending are controlled by means of a harmonic potential. For nonbonded, unlike pair interactions, Lorentz−Berthelot combining rules are used, which in previous work have been shown to be suitable for alkane mixtures.[27] In all calculations, a cutoff radius of 10.0 Å is employed for Lennard-Jones interactions and standard tail corrections[28,29] are implemented. The NERD force field has been shown to provide good agreement with experimental phase-equilibria data for pure alkanes and alkenes, and their binary and ternary mixtures.[20,23−25,27]

Table 1. Bonding and Nonbonding Potential Energy Functions and Parameters

Bond Stretching Potential

$U(r)/k_B = K_r/(r - b_{eq})^2$

$K_r = 96500\ K/Å^2$ | $b_{eq} = 1.54$ Å (C − C); $b_{eq} = 1.34$ Å (C = C)

Bond Bending Potential

$U(\theta)/k_B = K_\theta/2\ (\theta - \theta_{eq})^2$

$K_\theta = 62500\ K/rad^2$ | $\theta_{eq} = 114.0°$ (C − C − C); $\theta_{eq} = 124.0°$ (C − C = C); $\theta_{eq} = 109.4°$ (centered at CH(sp^3) branch unit)

Torsional Potential

$U(\phi)/k_B = U_0 + U_1(1 + \cos\phi) + U_2(1 - \cos 2\phi) + U_3(1 + \cos 3\phi)$

linear (C−C−C−C): $U_0 = 0$, $U_1 = 355.04$ K, $U_2 = -68.19$ K, $U_3 = 791.32$ K

linear (C−C−C═C): $U_0 = 47.97$ K, $U_1 = 86.31$ K, $U_2 = -109.71$ K, $U_3 = 282.08$ K

branched (C − C − C − C): $U_0 = 1416.30$ K, $U_1 = 398.30$ K, $U_2 = 139.12$ K, $U_3 = -901.20$ K

Nonbonded Interaction Potential:

$U(r) = 4\epsilon[(\sigma/r)^{12} - (\sigma/r)^6]$

Ethylene		
$\sigma_{CH_2(sp^2)} = 3.79$ Å	$\epsilon_{CH2(sp^2)} = 84.7$ K	
1-Hexene		
$\sigma_{CH_3(sp^3)} = 3.91$ Å	$\epsilon_{CH_3(sp^3)} = 104.0$ K	
$\sigma_{CH_2(sp^2)} = 3.72$ Å	$\epsilon_{CH_2(sp^2)} = 92.5$ K	(end group)
$\sigma_{CH_2(sp^3)} = 3.93$ Å	$\epsilon_{CH_2(sp^3)} = 45.8$ K	(middle group)
$\sigma_{CH(sp^2)} = 3.77$ Å	$\epsilon_{CH(sp^2)} = 46.0$ K	
Polyethylene Chains		
$\sigma_{CH(sp^3)} = 3.85$ Å	$\epsilon_{CH(sp^3)} = 39.7$ K	
$\sigma_{CH_2(sp^3)} = 3.93$ Å	$\epsilon_{CH_2(sp^3)} = 45.8$ K	
$\sigma_{CH_3(sp^3)} = 3.91$ Å	$\epsilon_{CH_3(sp^3)} = 104.0$ K	

2.2. Simulated LLDPE Chain Architectures. Two polyolefin architectures of 500 monomer backbone are studied to observe the effect of polymer chain branching on ethylene and 1-hexene solubilities. The first polymer architecture, linear C_{1000}, is composed of 100% ethylene repeat units and 1000 total united-atom sites. The second architecture, branched C_{1100}, is composed of 95% ethylene and 5% 1-hexene repeat units (1100 total united-atom sites). For branched C_{1100}, 1-hexene units are separated by 19 ethylene units in a chain (each chain having a total of 475 ethylene and 25 1-hexene units incorporated into the chain). The branching stereochemistry is not distinguished with the NERD force field.

2.3. Simulation Methods. Ethylene and 1-hexene solubility simulations are conducted using the recently proposed hyper-parallel tempering osmotic ($\mu_1...\mu_k N_{PE} pT$) ensemble technique.[1] In the osmotic ensemble, simulations are conducted with a constant number of polymer chains (N_{PE}) in a simulation cell at a given temperature (T), pressure (p), and chemical potential of the gases ($\mu_1...\mu_k$) that sorb into the polymer phase. The full details of this ensemble can be found in an earlier publication.[1] To characterize pure PE, isothermal−isobaric ensemble ($N_{PE}pT$) simulations have also been conducted. Sampling of phase space is achieved through Monte Carlo moves involving ethylene and/or 1-hexene insertion and deletion (for osmotic ensemble simulations only), volume changes, and site displacements at constant volume and number of molecules.

Constant volume molecular displacement moves include Hybrid-*NVT* (CVHMC) moves,[30,31] continuum configurational bias (CB)[32−34] moves, polymer chain CB reptation moves (for linear chains only), and CB inner chain rebridging moves.[35] The simulation cell volume fluctuates with reversible Berendsen Hybrid-*NPT* (CPHMC) moves.[36,37] The insertion and deletion of monomers into the simulation cell are conducted via a CB technique.

In addition to the osmotic and $N_{PE}pT$ ensemble formalisms, we have included a parallel tempering technique in our simulations.[38−40] Yan et al. studied Lennard-Jones atoms and polymeric systems in a grand canonical formalism[38,39] and found a speedup with the parallel tempering scheme. In this technique, N ensemble replicas are run independently using regular ensemble moves. Attempts are also made to exchange the extensive variables of two replicas with acceptance related to their partition functions. Each replica may be at different specified intensive variables (temperatures, pressures, and chemical potential(s) of gases for osmotic ensemble; temperature and pressure for NpT ensemble). However, the same extensive variables are kept constant in each replica (the number of molecules for the polymer is the same and constant for each replica in the osmotic ensemble formalism; the number of molecules for all components is the same and constant for each replica in the NpT ensemble formalism). For randomly chosen pairs, an exchange between replica configurations $\boldsymbol{x}_\mathbf{l}$ and $\boldsymbol{x}_\mathbf{m}$ is accepted according to

$$P_{\text{accept}}(\boldsymbol{x}_\mathbf{l} \leftrightarrow \boldsymbol{x}_\mathbf{m}) = \min\left[1, \frac{P_{\text{ensemble,l}}(\boldsymbol{x}_\mathbf{m}) P_{\text{ensemble,m}}(\boldsymbol{x}_\mathbf{l})}{P_{\text{ensemble,l}}(\boldsymbol{x}_\mathbf{l}) P_{\text{ensemble,m}}(\boldsymbol{x}_\mathbf{m})}\right] \quad (1)$$

where $P_{\text{ensemble,i}}(\boldsymbol{x}_\mathbf{j})$ is the probability of replica i having configuration $\boldsymbol{x}_\mathbf{j}$ for an arbitrary ensemble. For example, the following acceptance criteria for swapping osmotic ensemble replica configurations can be determined[1]

$$P_{\text{accept}}(\boldsymbol{x}_\mathbf{l} \leftrightarrow \boldsymbol{x}_\mathbf{m}) = \min[1, \exp(-\beta_\mathrm{l}\Delta U_\mathrm{l} - \beta_\mathrm{l} p_\mathrm{l} \Delta V_\mathrm{l} + \sum_{i=1}^{k} \beta_\mathrm{l} z_{i,\mathrm{l}}^{\text{mod}} \Delta N_{i,\mathrm{l}}) \times \exp(-\beta_\mathrm{m}\Delta U_\mathrm{m} - \beta_\mathrm{m} p_\mathrm{m} \Delta V_\mathrm{m} + \sum_{i=1}^{k} \beta_\mathrm{m} z_{i,\mathrm{m}}^{\text{mod}} \Delta N_{i,\mathrm{m}})] \quad (2)$$

where

$$\Delta A_\mathrm{m} = -\Delta A_\mathrm{l} = A(\boldsymbol{x}_\mathbf{m}) - A(\boldsymbol{x}_\mathbf{l}) \quad (3)$$

and A_j is a varying configurational dependent variable in replica j (e.g., the internal energy, U_j, the replica volume, V_j, or the number of molecules of type i, $N_{\mathrm{i,j}}$).

As mentioned above, gas-phase chemical potentials are required for the osmotic ensemble simulations. Gas-phase chemical potentials needed for the osmotic ensemble are calculated using a configurational bias test molecule insertion scheme within an NpT simulation[28] of the specified gas phase. The reduced chemical potential of molecule i, $\beta z_\mathrm{i}^{\text{mod}}$, is determined by[1]

$$z_\mathrm{i}^{\text{mod}} = \beta\mu_\mathrm{i} - \ln \lambda_\mathrm{i}^{3} + \ln C_{\text{chn i}} = \ln(N_\mathrm{i} + 1) - \ln\langle V W_{\text{test i}}^{\text{ext}} \rangle \quad (4)$$

where β is $1/k_\mathrm{B}T$, μ_i is the chemical potential of molecule i, λ_i is the de Broglie wavelength of component i, defined by $(\hbar/2\pi m_i k_\mathrm{B} T)^{1/2}$, m_i is the mass of component i, N_i is the number of i type molecules in the system, $W_{\text{test i}}^{\text{ext}}$ is the Rosenbluth weight[41] associated with a test molecule of type i inserted into the system, and $C_{\text{chn i}}$ is $\Pi_{j=1}^{n_\mathrm{i}} C_{\text{chn i,site j}}$, where $C_{\text{chn i,site j}}$ is given by

$$C_{\text{chn i,site j}} = \int \mathrm{d}\boldsymbol{r}\, \mathrm{e}^{-\beta U_{\text{chni,sitej}}^{\text{bonded}}(\boldsymbol{r})} \quad (5)$$

where $U_{\text{chn i,site j}}^{\text{bonded}}$ is the bonded (bond stretching, bond angle bending, and/or torsion) potential energy associated with the addition of site j of molecule type i and the integral is over all configurational phase space.

For this study, the reduced chemical potentials of ethylene in pure ethylene gas, 1-hexene in pure 1-hexene gas, and ethylene and 1-hexene in a 95 mol % ethylene/5 mol % 1-hexene gas mixture are determined for various conditions. NpT simulations consist of 80% constant volume CB moves and 20% random volume moves. Each CB move is performed using 10 trial orientations per site. Random volume moves are conducted with a maximum volume change of $10-100\sigma_{\text{LJ,min}}^{3}$ for the various conditions considered. All simulations are run for 5×10^6 steps with 200−400 molecules per simulation cell; 250 test molecule insertions are conducted every 10 steps in a configurational bias manner with 10 trial orientations per site. The average $VW_{\text{test i}}^{\text{ext}}$ is used with eq 4 to find the ethylene and/or 1-hexene reduced chemical potential for a given condition.

2.4. Simulation Specifications. For all polymer simulations, the simulation cell contains two polyolefin chains with initial configurations (for each condition) generated independently (using periodic boundaries). Each initial configuration is generated at random in a large simulation box (i.e., at low density). The system is then allowed to relax using NpT molecular dynamics simulations with the NERD united-atom force field, until an equilibrated state is reached for the configuration at the specified pressure and temperature. We have also studied systems of up to eight polyolefin chains, and the results for solubility are identical to those with two chains.

For the pure polyethylene $N_{PE}pT$ simulations, 10 $N_{PE}pT$ ensembles are run within the parallel tempering framework for PE modeled as linear C_{1000} with each ensemble at 1 bar and at temperatures ranging from 70 to 200 °C. For ethylene solubility simulations, 10 osmotic ($\mu_{\text{ethylene}}N_{PE}pT$) ensembles are run within the parallel tempering framework at temperatures ranging from 70 to 200 °C. For each polyethylene model, 3 of these simulations are conducted at 9.5, 19, and 30 bar. For 1-hexene solubility and ethylene/1-hexene co-solubility simulations, 15 osmotic ($\mu_{1-\text{hexene}}N_{PE}pT$ and $\mu_{\text{ethylene}}\mu_{1-\text{hexene}}N_{PE}pT$) ensembles are run within the parallel tempering framework at temperatures ranging from 70 to 200 °C. For each polyethylene model, 2 of these simulations are conducted at 0.5 and 1.0 bar for the 1-hexene solubility simulations. For the linear C_{1000} PE architecture, two ethylene/1-hexene co-solubility simulations are conducted at 10 and 20 with a specified gas-phase composition of 95 mol % ethylene and 5 mol % 1-hexene.

The full details of the solubility simulation conditions as well as the reduced chemical potentials determined by gas-phase simulations are provided in Tables 2 and 3. Details of the Monte Carlo (MC) move parameters

Table 2. Conditions for Ethylene/Polyethylene and 1-Hexene/Polyethylene Osmotic Ensemble Simulations[a]

ethylene solubility simulations						1-hexene solubility simulations			
9.5 bar systems		19 bar systems		30 bar systems		0.5 bar systems		1 bar systems	
T (K)	z_{eth}^{mod}	T (K)	z_{eth}^{mod}	T (K)	z_{eth}^{mod}	T (K)	z_{eth}^{mod}	T (K)	z_{eth}^{mod}
343	−8.5483	343	−7.8894	343	−7.4723	343	−11.677	343	−10.997
353	−8.5739	353	−7.9118	353	−7.4910	353	−11.689	353	−11.009
363	−8.5990	363	−7.9340	363	−7.5099	363	−11.702	363	−11.021
378	−8.6357	378	−7.9671	378	−7.5387	373	−11.714	373	−11.032
393	−8.6715	393	−7.9996	393	−7.5675	378	−11.720	378	−11.038
408	−8.7062	408	−8.0316	408	−7.5963	383	−11.727	383	−11.044
423	−8.7399	423	−8.0629	423	−7.6249	393	−11.739	393	−11.055
438	−8.7727	438	−8.0629	438	−7.6533	403	−11.751	403	−11.067
453	−8.8046	453	−8.0937	453	−7.6813	413	−11.764	413	−11.079
473	−8.8457	473	−8.1238	473	−7.7180	423	−11.776	423	−11.090
						433	−11.788	433	−11.102
						443	−11.801	443	−11.113
						453	−11.813	453	−11.125
						463	−11.825	463	−11.137
						473	−11.838	473	−11.148

[a] Reduced chemical potentials are determined for the pure gas at the specified temperature and pressure as described in section 2.3.

Table 3. Conditions for Ethylene/1-Hexene/Polyethylene Osmotic Ensemble Simulations[a]

10 bar systems			20 bar systems		
T (K)	z_{eth}^{mod}	z_{hex}^{mod}	T (K)	z_{eth}^{mod}	z_{hex}^{mod}
343	−8.5431	−11.8175	343	−7.8721	−11.339
353	−8.5664	−11.8137	353	−7.8939	−11.315
363	−8.5897	−11.8114	363	−7.9157	−11.294
373	−8.6130	−11.8107	373	−7.9375	−11.277
378	−8.6247	−11.8109	378	−7.9485	−11.270
383	−8.8114	−11.811	383	−7.9594	−11.263
393	−8.6596	−11.8132	393	−7.9812	−11.253
403	−8.6829	−11.8162	403	−8.0030	−11.245
413	−8.7062	−11.8202	413	−8.0248	−11.239
423	−8.7295	−11.8250	423	−8.0466	−11.235
433	−8.7528	−11.8368	433	−8.0685	−11.233
443	−8.7762	−11.8368	443	−8.0903	−11.232
453	−8.7995	−11.8434	453	−8.1121	−11.232
463	−8.8228	−11.8505	463	−8.1339	−11.233
473	−8.8461	−11.8577	473	−8.1557	−11.234

[a] In all cases, reduced chemical potentials are calculated for gases of 95 mol % ethylene/5 mol % 1-hexene.

Table 4. Parameters Used for Monte Carlo Moves[a]

MC move	no. of sites/ move[b]	no. of trial insertions/ site	no. of MD steps per move	reduced MD time step[c]
		CB Moves		
ethylene insertion/deletion	2	15[d] 20[e]		
1-hexene insertion/deletion	6	20		
chain end-site[f]	1−6 (PE) 1−2 (ethylene) 1−6 (1-hexene)	10		
branch end-site[g]	1−4 (PE)	10		
reptation[h]	1−4 (PE)	10		
inner chain rebridging	2−6 (PE)	10		
		Hybrid-MC Moves		
CPHMC			15	0.001
CVHMC			15	0.018

[a] For moves with parameters different for ethylene, 1-hexene, and polyethylene, the molecule for the parameter is specified in parentheses. [b] Randomly chosen between given range. [c] Reduced in terms of σ, ϵ, and the mass of the Lennard-Jones site with minimum σ. [d] For binary ethylene/PE simulations. [e] For ternary ethylene/1-hexene/PE simulations. [f] End-chain CB method for 2 ends of the chain. [g] End-chain CB for branches in the chain (only for branched C_{1100}). [h] Only for linear C_{1000}.

and simulation specifications for the osmotic and $N_{PE}pT$ simulations are provided in Tables 4 and 5.

3. Equations of State Modeling

For phase equilibrium, the temperature, pressure, and component chemical potentials are equivalent in the vapor (V) and amorphous polymer (amph P) phases. In this work the vapor phase pressure and chemical potentials are modeled with the perturbed-chain statistical associating fluid theory (PC−SAFT) equation of state.[2−4]

$$P^{V} = P^{V,res,PC-SAFT} + P^{IG} \tag{6}$$

$$\mu_i^{V,res} = \mu_i^{V,res,PC-SAFT} \tag{7}$$

where i is an index for gas i in the mixture (ethylene or 1-hexene in this work). It is assumed that the concentration of polymer in the gas phase is negligible.

Above the polymer melting point, the purely amorphous polymer phase pressure and chemical potentials are also modeled with the PC−SAFT equation of state.

$$P^{pure\ amph\ P} = P^{pure\ amph\ P,res,PC-SAFT} + P^{IG} \tag{8}$$

$$\mu_i^{pure\ amph\ P,res} = \mu_i^{pure\ amph\ P,res,PC-SAFT} \tag{9}$$

Below the melting point, real polyolefins exhibit a semicrystalline structure. This structure restricts polymer swelling and inhibits gas sorption in the amorphous polymer phase of the semicrystalline polyolefin (it is assumed that no gas sorbs into the crystalline phase of polyolefin). Our molecular simulations and the PC−SAFT equation of state do not account for this elastic effect of gas sorption in the amorphous polymer phase. A model has therefore been adopted to account for these elastic constraints through a modified expression for pressure and chemical potential:

$$P^{amph\ P} = P^{pure\ amph\ P} + P^{amph\ P,elastic} \tag{10}$$

$$\mu_i^{amph\ P,res} = \mu_i^{pure\ amph\ P,res} + \Delta\mu_i^{amph\ P,elastic} \tag{11}$$

Equations 6−11 form the basis for the phase equilibria calculations. Some details pertaining to each of the terms appearing in these equations are provided below.

Table 5. Simulation Specifications for Osmotic and $N_{PE}pT$ Ensemble Simulations[a]

Distribution of Monte Carlo Moves

		distribution of non-PT swapping MC moves							
gas/PE models	% PT swapping	% CPHMC	% CVHMC	% ethylene/ 1-hexene CB insertion/ deletion	% chain end-site CB	% branch end-site CB	reptation	% inner chain rebridging	no. of MC steps/system ($\times 10^{-6}$)
				Osmotic Simulations					
ethylene/linear C_{1000}	0.05	1	0.25	83	1.25		4.5	10	5 (9.5, 19 bar) 8 (30 bar)
1-hexene/linear C_{1000}	0.02	1	0.25	83	1.25		4.5	10	5 (0.5 bar)
ethylene/1-hexene/linear C_{1000}	0.02	1	0.25	83	1.25		4.5	10	20 (10, 20 bar)
ethylene/branched C_{1100}	0.05	1	0.25	83	0.575	5.175		10	10 (9.5 bar) 5 (19, 30 bar)
1-hexene/branched C_{1100}	0.02	1	0.25	83	0.575	5.175		10	5 (0.5 bar) 10 (1 bar)
				$N_{PE}pT$ Simulations					
linear C_{1000}	0.05	0.8	0.2	10			43	46	2 (1 bar)

Monte Carlo Move Acceptances[b]

% PT swapping	% CPHMC	% CVHMC	% ethylene CB insertion/deletion	% 1-hexene CB insertion/deletion	% end-site CB[c]	% reptation CB	% inner chain rebridging
10−20	20−30	50−70	2−20	0.1−5	30−50	5−15	3−6

[a] The distribution of Monte Carlo moves for each simulation and general Monte Carlo move acceptances are indicated in the table. For the distribution of Monte Carlo moves, the mixtures studied are shown in the left-hand column. Distinctions between the different pressures studied for a given mixture are indicated in parentheses. [b] Range of acceptances for all simulations. For non-PT swapping moves, acceptances are generally insensitive to pressure, higher for higher temperature conditions, and lower for lower temperature conditions. [c] Overall acceptance for chain and branch end-site CB moves.

3.1. PC−SAFT Equation of State. The PC−SAFT residual Helmholtz free energy depends on the mole fraction (x_i) of each species, the total number of moles in the system (n), the system volume (V), and system temperature (T) and is modeled as

$$A^{\text{res,PC-SAFT}}(x_i,n,V,T) = A^{\text{hs}}(x_i,n,V,T) + A^{\text{chain}}(x_i,n,V,T) + A^{\text{assoc}}(x_i,n,V,T) + A^{\text{disp}}(x_i,n,V,T) \quad (12)$$

where A^{hs} represents a hard-sphere contribution, A^{chain} is the contribution of bonding of the spherical sites to form chains, A^{assoc} accounts for association between nonbonded sites (eg. hydrogen bonding), and A^{disp} is a dispersion contribution. For our systems, A^{assoc} is equal to zero as there is no association between nonbonded sites in the mixtures we study here. The dispersion term is different in the PC−SAFT and the original SAFT model. The PC−SAFT model is adopted here due to its improved performance over the conventional SAFT model. Full details can be found in the original references.[2−7]

Molecule-specific parameters appearing in PC−SAFT include a temperature independent segment diameter, $\sigma_i^{\text{PC-SAFT}}$, the number of segments per molecule, m_i, the molecule molecular weight, MW_i, and a segment energy, $\epsilon_i^{\text{PC-SAFT}}$. For unlike pair interactions between type i and j sites (appearing in the dispersion contribution of PC−SAFT), the effective interaction diameter is given by $\sigma_{ij}^{\text{PC-SAFT}} = {}^1/_2(\sigma_i^{\text{PC-SAFT}} + \sigma_j^{\text{PC-SAFT}})$ and the energy of interaction is given by $\epsilon_{ij}^{\text{PC-SAFT}} = (1 - k_{ij})(\epsilon_i^{\text{PC-SAFT}}\epsilon_j^{\text{PC-SAFT}})$, where an adjustable binary interaction parameter, k_{ij}, has been introduced.

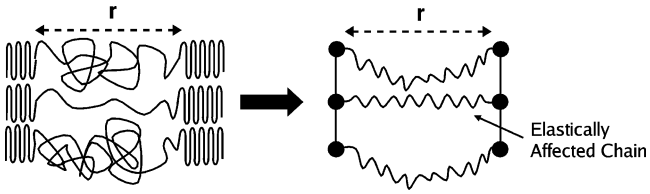

Figure 1. Illustration of elastic effect in a semicrystalline polymer.

The pressure and residual chemical potentials for each species are found through the following thermodynamic definitions

$$P^{\text{res,PC-SAFT}} \equiv \left(\frac{\partial A^{\text{res,PC-SAFT}}}{\partial V}\right)_{N,T} \quad (13)$$

$$\mu_i^{\text{res,PC-SAFT}} \equiv \left(\frac{\partial A^{\text{res,PC-SAFT}}}{\partial N_i}\right)_{N_{j\neq i},T,V} \quad (14)$$

3.2. Elastic Constraints. To describe the elastic contributions appearing in eqs 10 and 11, we have implemented a model akin to those proposed by Flory and Michaels et al. and Rogers and Doong et al.[9,10,42,43] Consider the cartoon of a semicrystalline polymer depicted in Figure 1. In this model, polymer swelling in an amorphous interphase region (the amorphous interphase region refers to the amorphous polymer domains that exist between adjoining crystalline regions) is constrained by stretching constraints exerted by "elastically affected" tie segments between crystallites. In this model, the free energy associated with the stretching of "elastically affected" tie segments is described by

$$\Delta U^{\text{amph P,elastic}} = Kr^2/2u \quad (15)$$

where $\Delta U^{\text{amph P,elastic}}$ is the elastic energy (per methyl unit in tie segment) associated with the stretching of "elastically affected" chains and r is the average distance between adjoining crystallites of an "elastically affected" chain. This energy is assumed to follow a Hookean form characterized by a spring constant K, and the average number of methyl units in the tie segments u. The fraction of "elastically affected" chains in the amorphous interphase, f, is defined by

$$\frac{\nu u}{N_A} = f n_P \tag{16}$$

where ν is the total number of polymer tie segments in the amorphous interphase region, N_A is Avogadro's number, and n_P is the total number of moles of polymer in the amorphous polymer interphase.

By making use of general thermodynamic relationships and the melting point depression of a crystalline polymer by a solvent, the following expressions are obtained for the elastic contribution on the solvent i chemical potential in the amorphous polymer phase and polymer phase pressure (see Supporting Information):

$$\Delta\mu_i^{\text{amph P,elastic}}/RT = \frac{\frac{\bar{v}_i^{\text{amph P}}}{\bar{v}_P^{\text{amph P}}}\left[\frac{\Delta H_{\text{fusion}}}{R}\left(\frac{1}{T}-\frac{1}{T_m}\right)+\mu_P^{\text{pure amph P,res}}/RT\right]}{\frac{3}{2f\phi_P^{\text{amph P}}}-1} \tag{17}$$

$$P^{\text{amph P,elastic}} = -3\left(\frac{RT}{\bar{v}_P^{\text{amph P}}}\right)\frac{\left[\frac{\Delta H_{\text{fusion}}}{R}\left(\frac{1}{T}-\frac{1}{T_m}\right)+\mu_P^{\text{pure amph P,res}}/RT\right]}{\frac{3}{2f\phi_P^{\text{amph P}}}-1} \tag{18}$$

where T_m is the melting temperature (determined from DSC measurements), $\bar{v}_i^{\text{amph P}}$ is the partial molar volume of species i in the amorphous polymer phase (calculated from simulations as described in a previous publication[1]), and $\phi_P^{\text{amph P}}$ is the volume fraction of the polymer in the amorphous polymer phase.

We are not aware of any previous results quantifying the fraction of "elastically affected" chain parameter, f, for a given polymer sample. However, we believe that it is possible to obtain a value for f based on experimental studies of "constrained interphases" in the manner proposed by previous investigations.[12−14] In addition, it may be possible to measure this parameter with improved molecular simulation techniques in the future.

4. Experimental LLDPE Samples

Table 6 summarizes the properties of the LLDPE samples for which experimental solubility results are used to compare with our model results.

The samples were prepared by polymerization in a gas-phase stirred bed reactor over a Ziegler−Natta type catalyst at 8.27 bar and 70 °C. To produce PE388 and PE475, ethylene was copolymerized at 2.00 and 3.25 mol % 1-hexene in the gas phase. The sample melting points and heats of fusion were characterized by differential scanning calorimetry (DSC) analysis. The crystallinity was determined based on the measured heats of fusion.

Table 6. Characterization of Poly(ethylene-*co*-1-hexene) Samples from Novak et al.,[22] Where Crystallinity Data Is Based on a Value for the Heat of Fusion of 100% Crystalline PE of 280−290 J/g.

sample	1-hexene (mol % in PE)	T_{melt} (°C)	heat of fusion (J/g)	% crystallinity
PE000	0	142.9	202.3	69.7−72.3
PE388	3.88	139.3	180.0	62.0−64.3
PE475	4.75	138.2	171.2	59.0−61.2

The sorption measurements were conducted at 70, 90, and 150 °C using a Rubotherm magnetic suspension balance in a high-pressure vessel under specified temperatures and pressures. For this work, the gas sorption measurements are reported on the basis of gas solubility per gram of amorphous polymer assuming no gas sorbs into the crystalline polymer phase for experiments performed with semicrystalline polymer (below the polymer melting temperature). For the sorption measurements below the polymer melting temperature (70 and 90 °C, it is assumed that the polymer crystallinity does not change with gas sorption (i.e., it is assumed that no "partial melting" of crystallites occurs due to the presence of solvent at these conditions). Previous investigations of gas sorption for various alkenes and aromatics in polyethylene suggest that "partial melting" of semicrystalline polyethylene due to the addition of solvent will not be significant at temperatures below 100 °C.[9,44,45] The full details of the experimental procedures can be found in the original reference, ref 22.

5. Results and Discussion

5.1. PC−SAFT Parametrization. PC−SAFT parameters for ethylene and 1-hexene are taken from the original publication.[2] We note here that with the original parametrization, the predictions of PC−SAFT for liquid density deviate slightly from those of molecular simulations, thereby leading to slight discrepancies in the ensuing solubility predictions. To arrive at better equation-of-state parameters for linear C_{1000}, NpT simulations of pure linear C_{1000} were conducted. The resulting densities are shown in Figure 2. As observed in

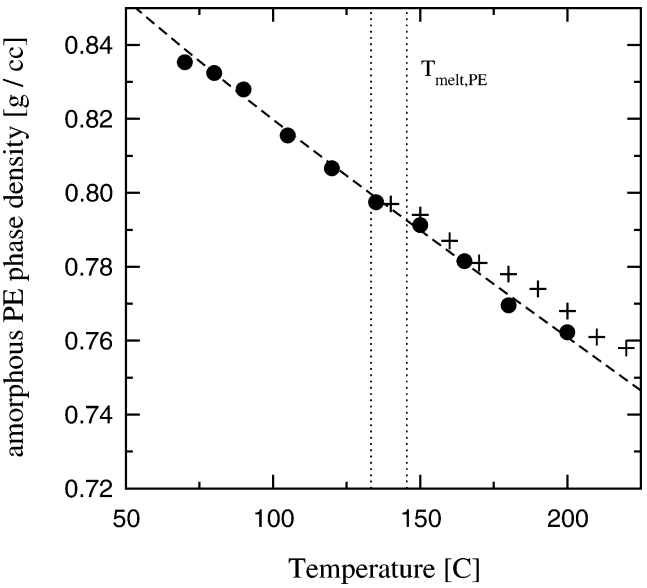

Figure 2. Density of pure linear C_{1000} at 1 bar: (●) simulation results; (+) experimental results[46] for a purely amorphous high-density polyethylene (M_n = 28K, M_w/M_n = 4.5). The dashed line (- -) is the PC−SAFT fit to the simulation results.

Table 7. PC−SAFT Parameterization

PC−SAFT Pure Component Parameters				
	MW (g/mol)	m	σ (Å)	ϵ/k_B (K)
ethylene	28.054	1.5930	3.4450	176.47
1-hexene	84.161	2.9853	3.7753	236.81
linear C_{1000}	14029	369.50	3.9876	246.0

Binary Interaction Parameters

$k_{eth-linC_{1000}} = 0.000$

$k_{hex-linC_{1000}} = 0.000$

$k_{eth-hex} = 0.000$

Figure 2, the results agree well with experimental data. The PC−SAFT parametrization is conducted with the same procedure proposed by Gross et al.[3] The number of segments in a polyethylene chain, m, is set to the value used by Gross et al. for all polyethylene models (reported as m/polymer molecular weight in the work of Gross et al.[3]). The segment diameter, σ, is modified from the value of Gross et al.[3] in order to obtain good agreement with simulated pure linear C_{1000} density results. As noted in the publication of Gross et al., the pure component density is insensitive to the segment dispersion energy term, ϵ/k_B. Ideally one would use vapor pressure data to fit ϵ/k_B. Such data, however, are not available for pure polyethylene; the segment dispersion energy term is therefore adjusted from the value originally proposed by Gross et al. by co-currently fitting PC−SAFT to *simulated* pure linear C_{1000} density and ethylene sorption in linear C_{1000} (results for ethylene sorption are given in the next section). In addition, the PC−SAFT binary interaction parameters k_{ij} are set to zero for all mixture calculations. As shown in the following sections, k_{ij} is not necessary to provide results that are consistent with those of our simulations of solubility. The full PC−SAFT parametrization for this work is provided in Table 7.

5.2. Ethylene Sorption in LLDPE. Figure 3 shows simulated ethylene solubility results in PE at 9.5, 19, and 30 bar and temperatures from 70 to 200 °C for

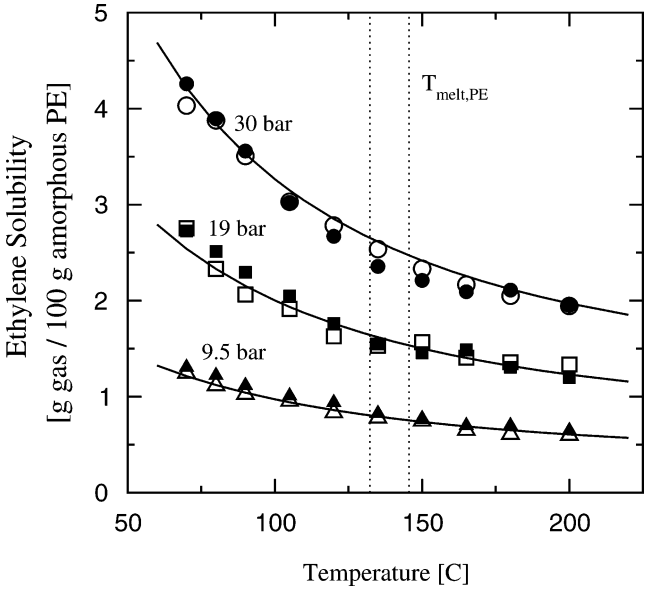

Figure 3. Simulated ethylene solubility in polyethylene with various polyethylene models: (▲, ■, and ●) simulated results for polyethylene modeled as linear C_{1000} at 9.5, 19, and 30 bar, respectively; (△, □, and ○) simulated results for polyethylene modeled as branched C_{1100} at 9.5, 19, and 30 bar, respectively. The solid curves (−) are the PC−SAFT predictions for ethylene solubility in linear C_{1000}.

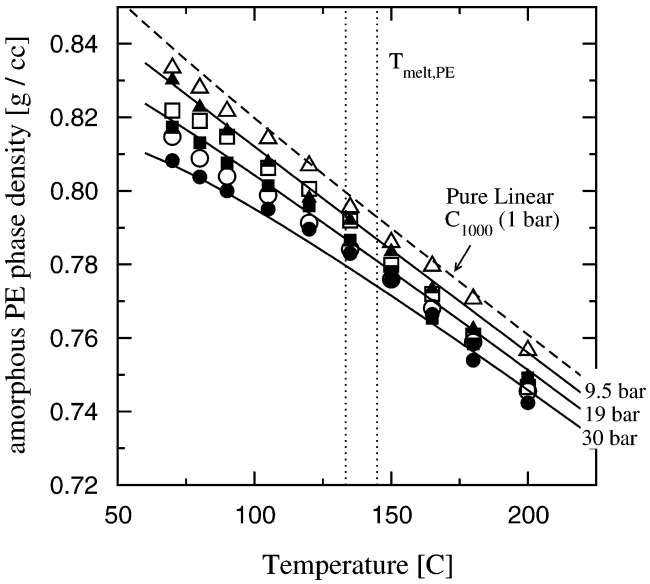

Figure 4. Simulated amorphous polymer phase density for ethylene/polyethylene mixture using various polyethylene models: (▲, ■, and ●) simulated results for polyethylene modeled as linear C_{1000} at 9.5, 19, and 30 bar, respectively; (△, □, and ○) simulated results for polyethylene modeled as branched C_{1100} at 9.5, 19, and 30 bar, respectively. The solid curves (−) are the PC−SAFT predictions for the ethylene/linear C_{1000} mixtures. The dashed curve (- -) is the PC−SAFT prediction for pure linear C_{1000} at 1 bar.

various chain architectures. No effect of short-chain branching is observed in the simulated results. This is consistent with the experimental observations of Novak et al.[22] as well as our previous results.[1] PC−SAFT ethylene solubility predictions in linear C_{1000} are also shown in Figure 2. PC−SAFT and simulated ethylene sorption predictions are within 10% for all conditions.

Figure 4 shows the corresponding simulated ethylene/PE mixture densities. As observed in the Figure, short chain branching has a tendency to increase the mixture densities, consistent with previous observations.[1] Upon comparison with pure unswollen linear C_{1000} at 1 bar, polyethylene swells with the addition of the lighter ethylene, as indicated by the reduction in density with increasing ethylene sorption (increasing ethylene sorption is indicated by the increasing pressures in the ethylene/polyethylene mixture densities shown in Figure 4). As Figure 4 shows, the PC−SAFT predicted ethylene/linear C_{1000} mixture densities agree relatively well with simulations (PC−SAFT and simulated ethylene/linear C_{1000} mixture density predictions are within 2% for all conditions). These findings indicate that PC−SAFT effectively captures the ethylene/PE mixture with regards to the predicted ethylene solubilities and polymer phase densities without the need for adjustable binary ethylene − PE interaction parameters.

As previously mentioned, both our molecular simulations and PC−SAFT predictions do not account for inherent elastic effects present within semicrystalline PE. Figure 5 shows the effect of elastic constraints on ethylene solubility in PE for 9.5, 19, and 30 bar. Partial molar volumes of 65 and 17000 cm^3/mol for ethylene and polyethylene modeled as linear C_{1000}, respectively, are assumed for eqs 17 and 18 to calculate the elastic contribution. The partial molar volumes are obtained from simulations at conditions below the polymer melting temperature (see ref 1). The heat of fusion for crystallites and the homopolymer melting temperature

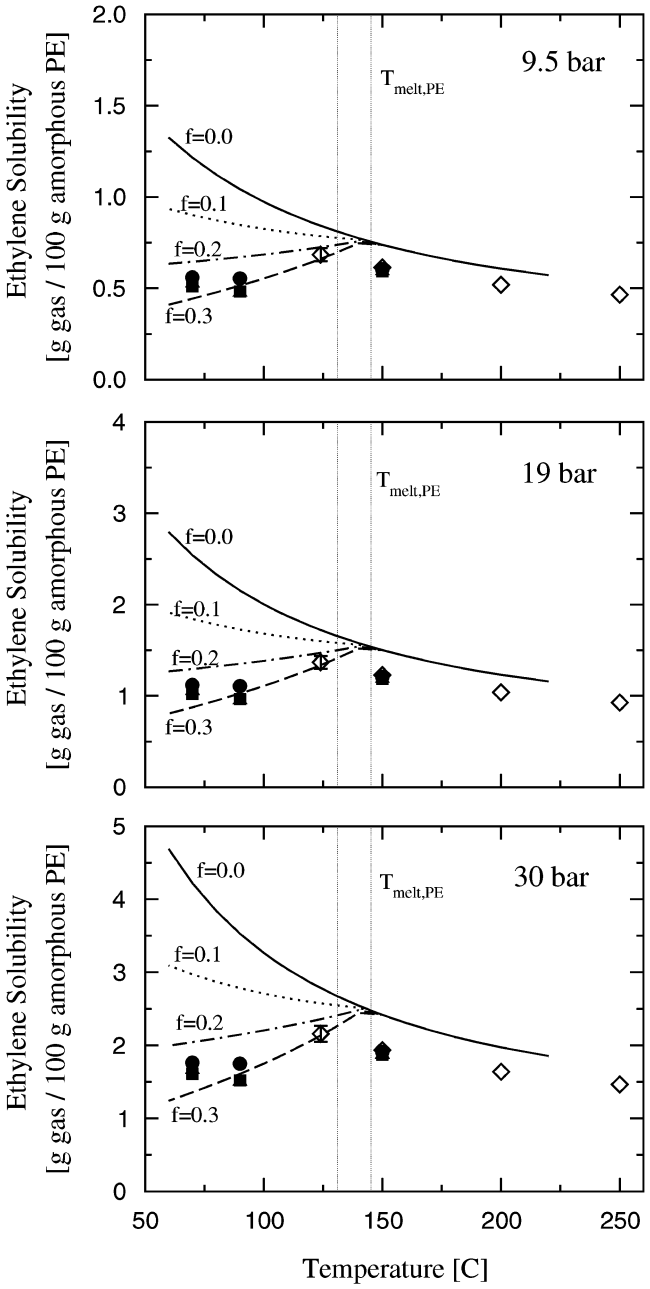

Figure 5. Elastic effect on ethylene solubility in linear C_{1000} at 9.5, 19, and 30 bar. The solid curves (—) are PC−SAFT results with no elastic effect, i.e., $f = 0.0$ (PC−SAFT fitted to simulation results). The dotted (···), dash−dotted (-·-), and dashed (- -) curves are PC−SAFT results corrected for elastic constraints with $f = 0.1$, $f = 0.2$, and $f = 0.3$, respectively. ●, ■, and ▲ are experimental ethylene solubility results in ethylene-1-hexene copolymers of 100, 96.12, and 95.25 mol % ethylene incorporated in the polyolefin (PE000, PE388, and PE475 from Table 6), respectively from Novak et al.[22] ◇ are experimental ethylene solubilities in a low-density polyethylene from Maloney et al.[47]

for eqs 17 and 18 are provided in Table 6. Experimental results for the polyethylene with 0−4.75% 1-hexene incorporated in the polymer are also shown in Figure 5. At temperatures above the melting point, there are no elastic effects and we observe that the molecular-simulation-fitted PC−SAFT curve slightly overpredicts the experimental results. For temperatures below the melting point, elastic effects are important. Upon melting, the experimentally observed ethylene solubility (per gram of amorphous polymer) increases considerably (In the absence of elastic effects, ethylene solubility would decrease with an increase in temperature). The inclusion of elastic constraints captures the experimentally observed decrease of ethylene in semicrystalline polyethylene when the fraction of "elastically affected" chains, f, is approximately 0.2−0.3. Also note that experimental results indicate that short-chain branching does not have an effect on ethylene solubility, consistent with our predictions. This experimental observation is confirmed for additional operating conditions in the work of Novak et al.[22]

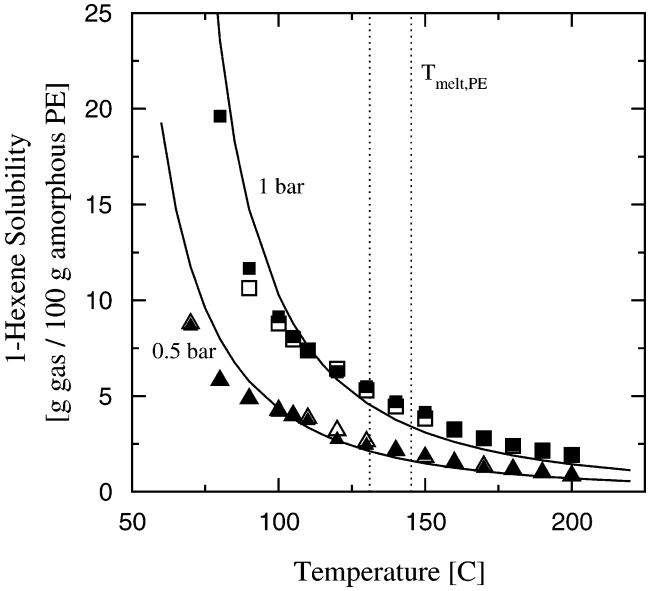

Figure 6. Simulated 1-hexene solubility in polyethylene with various polyethylene models: (▲ and ■) simulated results for polyethylene modeled as linear C_{1000} at 0.5 and 1 bar, respectively; (△ and □) simulated results for polyethylene modeled as branched C_{1100} at 0.5 and 1 bar, respectively. The solid curves (—) are the PC−SAFT predictions for 1-hexene solubility in linear C_{1000}.

5.3. 1-Hexene Sorption in LLDPE. Figure 6 shows our simulated 1-hexene solubility results in PE at 0.5 and 1 bar and temperatures from 70 to 200 °C for various chain architectures. As with the case of ethylene sorption, no effect of short-chain branching is observed. This is consistent with the experimental observations of Novak et al.[22] The PC−SAFT calculations agree well with simulated 1-hexene solubility predictions for the higher temperatures. However, a slight discrepancy is observed for temperatures below 100 °C. At these lower temperatures, PC−SAFT overpredicts 1-hexene solubilities compared to the simulations.

Figure 7 shows the corresponding simulated 1-hexene/PE mixture densities. As observed in Figure 7, short-chain branching has a tendency to increase the mixture densities. Another interesting observation is that swelling becomes increasingly important at lower temperatures. In fact, swelling becomes so dramatic that, below 100 °C, the density actually decreases with lower temperatures. PC−SAFT predictions agree relatively well with simulated densities for higher temperature simulations. However, some discrepancies can be seen in the results for temperatures below 100 °C. Since PC−SAFT overpredicts 1-hexene solubility at lower temperatures, more of the lighter 1-hexene is present in the polymer phase, thereby leading to the larger extent of swelling observed at these lower temperatures (see Figure 7).

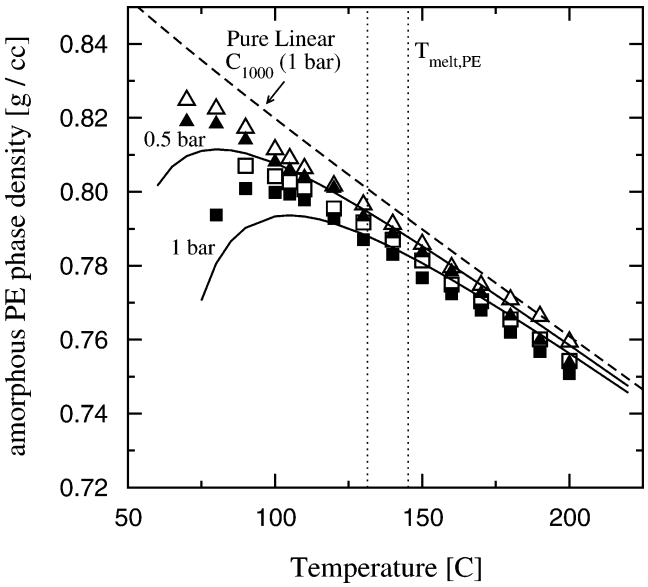

Figure 7. Simulated amorphous polymer phase density for 1-hexene/polyethylene mixtures for various polyethylene models: (▲ and ■) simulated results for polyethylene modeled as linear C_{1000} at 0.5 and 1 bar, respectively; (△ and □) simulated results for polyethylene modeled as branched C_{1100} at 0.5 and 1, respectively. The solid curves (—) are the PC−SAFT predictions for the 1-hexene/linear C_{1000} mixtures. The dashed curve (- - -) is the PC−SAFT prediction for pure linear C_{1000} at 1 bar.

Figure 8 shows the effect of elastic constraints on 1-hexene solubility in PE for 0.5 and 1 bar. Partial molar volumes of 130 and 17000 cm^3/mol for 1-hexene and polyethylene modeled as linear C_{1000}, respectively, are assumed for eqs 17 and 18 to calculate the elastic contribution. The partial molar volumes are extracted from simulations, as in the ethylene solubility case. The heat of fusion for crystallites and the homopolymer melting temperature for eqs 17 and 18 are provided in Table 6. Experimental results for the polyethylene with 0−4.75% 1-hexene incorporated in the backbone are also shown in Figure 7. For temperatures above the melting point, elastic effects are absent and the molecular-simulation-fitted PC−SAFT predictions agree well with experimental data. For temperatures below the melting point, elastic effects become significant. The molecular-simulation-fitted PC−SAFT curve without elastic effects greatly overpredicts the experimental solubility results. However, with the inclusion an elastic constraint, the experimental results can be described reasonably well. It is found that a similar elasticity effect ($f = 0.2$) as that required to describe ethylene/polyethylene mixtures provides an accurate representation of these systems. In addition, experimental results suggest that the effect of short-chain branching on 1-hexene solubility is negligible, consistent with our simulation observations. The reader is referred to experimental results at more operating conditions in the work of Novak et al.[22] for further information on this point.

5.4. Ethylene/1-Hexene Cosorption in LLDPE. Figure 9 shows our simulated solubility results for ternary mixtures of ethylene, 1-hexene, and polyethylene modeled as linear C_{1000} at 10 and 20 bar and temperatures from 70 to 200 °C. PC−SAFT fitted results are also shown in the Figure. For the ternary mixtures, the gas-phase composition is 95 mol % ethylene/5 mol % 1-hexene. Ethylene, 1-hexene, and total gas solubility results are shown in the Figure, along with results for binary mixtures (shown for comparison).

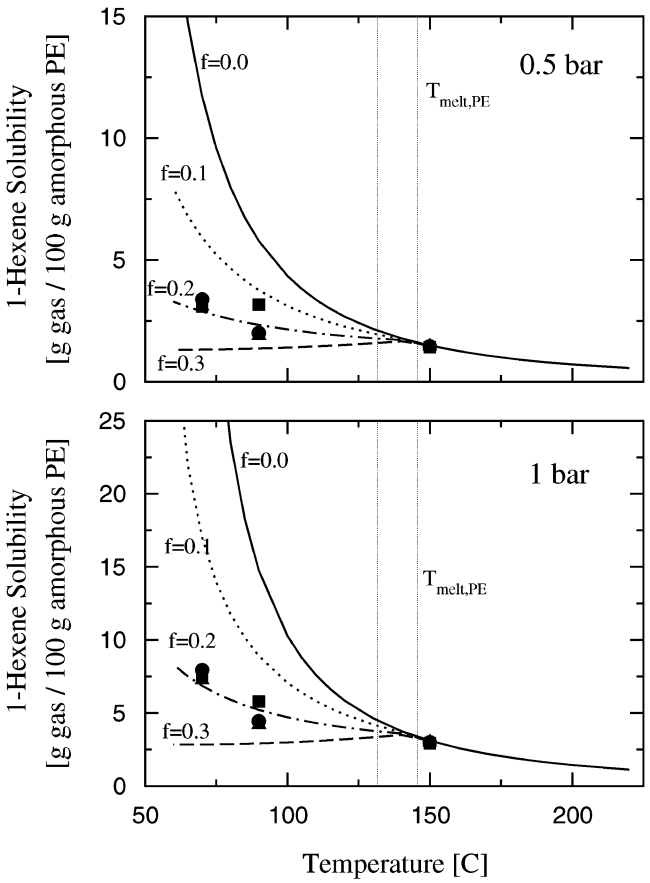

Figure 8. Elastic effect on 1-hexene solubility in linear C_{1000} at 0.5 and 1 bar. The solid curves (—) are PC−SAFT results with no elastic effect, i.e., $f = 0.0$ (PC−SAFT fitted to simulation results). The dotted (···), dash−dotted (-·-), and dashed (- -) curves are PC−SAFT results corrected for elastic constraints with $f = 0.1$, $f = 0.2$, and $f = 0.3$, respectively. ●, ■, and ▲ are experimental 1-hexene solubility results in ethylene-1-hexene copolymers of 100, 96.12, and 95.25 mol % ethylene incorporated in the polyolefin (PE000, PE388, and PE475 from Table 6), respectively from Novak et al.[22]

The corresponding ternary mixture densities are shown in Figure 10. It is observed that ethylene solubility is enhanced by the addition of 1-hexene to the gas phase. This is consistent with previous observations.[21] The addition of 1-hexene causes the amorphous polymer phase to be significantly more swollen than in the binary ethylene/amorphous polyethylene case (see the mixture densities shown in Figures 4 and 10). The PC−SAFT predicted swelling is large at lower temperatures due to the tendency of PC−SAFT to overpredict the solubility of 1-hexene in polyethylene at lower temperatures. It is also observed that 1-hexene solubility decreases with the addition of ethylene to the gas phase. Contrary to 1-hexene, ethylene does not swell polyethylene to a large extent, and therefore ethylene molecules tend to occupy the space that 1-hexene would normally occupy in a binary mixture, leading to a decrease in 1-hexene solubility with the inclusion of ethylene. The overall gas solubility in polyethylene is also reported in Figure 9. It is observed that the overall gas solubility decreases below the amount corresponding to the sum of the binary solubility results. When the ternary and binary mixtures are compared, it is seen that the decrease in 1-hexene solubility is greater in magnitude than the increase in ethylene solubility. Overall, PC−SAFT with fitted interaction parameters predicts the

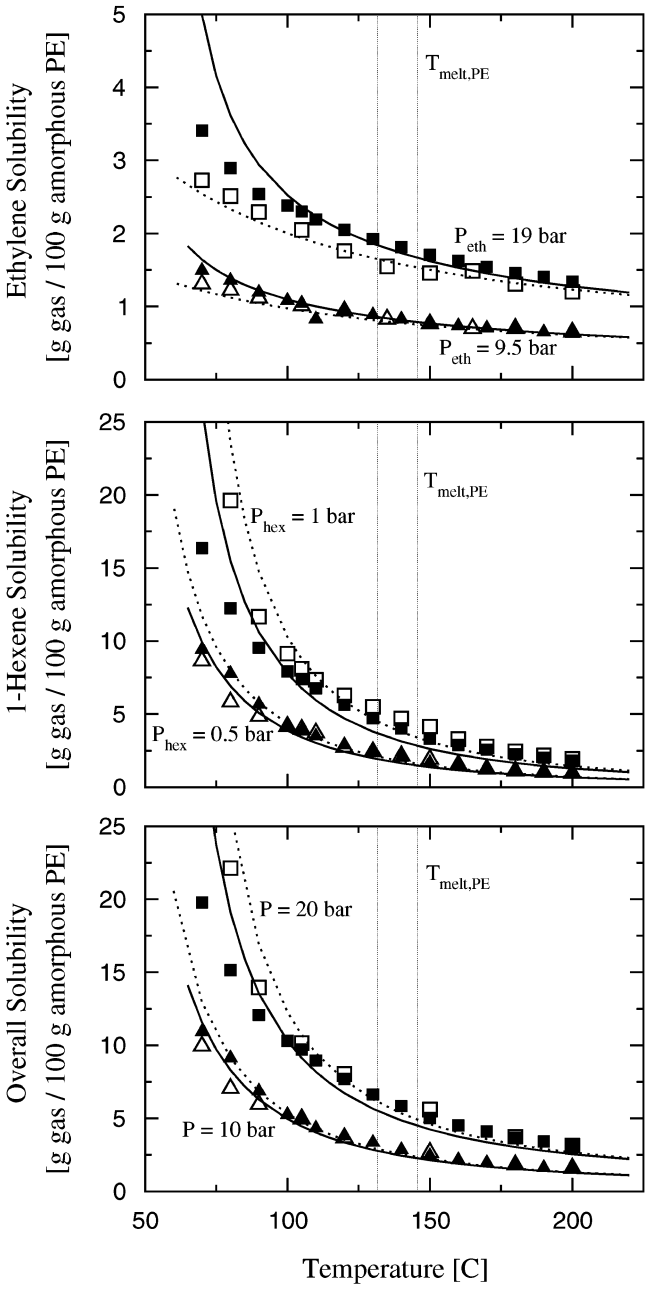

Figure 9. Simulated gas solubilities in polyethylene modeled as linear C_{1000} in ternary mixtures of ethylene/1-hexene/linear C_{1000}. The gas-phase composition is specified at 95 mol % ethylene/5 mol % 1-hexene for all conditions. ▲ and ■ are simulated results for solubilities in the ternary mixture at total pressures of 10 and 20 bar, respectively. △ and □ are simulated results for solubilities in binary monomer/polymer mixtures. The binary mixture overall solubiliry results are the sum of binary ethylene and 1-hexene solubilities at the ternary mixture conditions. The solid curves (—) are the PC−SAFT predictions for solubilities in the ternary mixture. The dotted curves (···) are the PC−SAFT predictions for solubilities in the binary monomer/polymer mixtures. The binary mixture overall solubility PC−SAFT predictions are the sum of binary ethylene and 1-hexene solubilities at the ternary mixture conditions.

same qualitative and quantitative behavior as the simulations. High-temperature results are in good agreement with simulation results, whereas the lower temperature predictions tend to overpredict the monomer solubilities, as is the case with the 1-hexene/polyethylene mixtures.

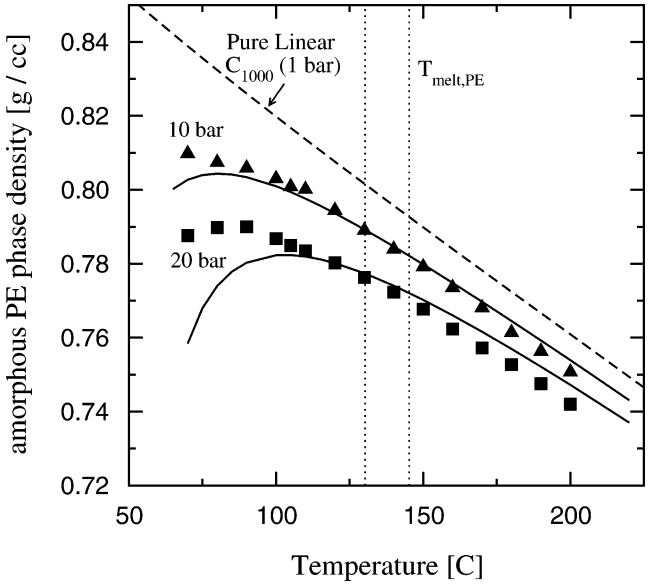

Figure 10. Simulated amorphous polymer phase density for the ethylene/1-hexene/linear C_{1000} mixture. The gas-phase composition is specified at 95 mol % ethylene/5 mol % 1-hexene for all conditions. ▲ and ■ are simulated results at total pressures of 10 and 20 bar, respectively. The solid curves (—) are PC−SAFT predictions for the ternary mixtures. The dashed curve (- -) is the PC−SAFT prediction for pure linear C_{1000} at 1 bar.

Figure 11 shows the effect of elastic constraints on ternary mixture solubilities in PE for 10 and 20 bar. The same values as for binary mixtures are used for the partial molar volumes, polyethylene crystallite heat of fusion, and polyethylene melting point in eqs 17 and 18 to calculate the elastic contribution. Ethylene, 1-hexene, and total gas solubility results are shown in Figure 11. The results for binary mixtures are included for comparison. Experimental total solubility data for polyethylene with 0−4.75% 1-hexene incorporated in the polymer are also shown in Figure 11. For temperatures above the melting point, elastic effects are absent, and the molecular simulation fitted PC−SAFT curve agrees well with experimental data for overall solubility. For temperatures below the melting point, elastic effects become significant. The molecular simulation fitted PC−SAFT curve without elastic terms overpredicts the experimental overall solubility results. The inclusion of an elastic constraint improves agreement with overall solubility measurements. A similar elasticity effect ($f = 0.2$) as that used for the binary ethylene and 1-hexene solubility gives a good representation of the ternary system's behavior. The experimental data indicate that short-chain branching does not influence the overall solubility, consistent with our binary mixture results.

It has previously been noted[15,16,18] that including 1-hexene in the ethylene gas phase leads to an enhancement in the polymerization reaction rate in olefin polymerization reactors—the so-called "comonomer effect" (results vary from no enhancement to up to a 4-fold increase of the polymerization rate, depending on the reactor conditions and type of catalyst). The origins of this effect are not completely understood. Some of the hypotheses put forward to explain this observation include the following: (1) 1-hexene changes the chemical nature of the catalyst as to enhance the polymerization reaction rate, (2) the enhanced swelling with the inclusion of 1-hexene increases the monomer diffusivity, thereby enhancing the apparent reaction rate, and (3)

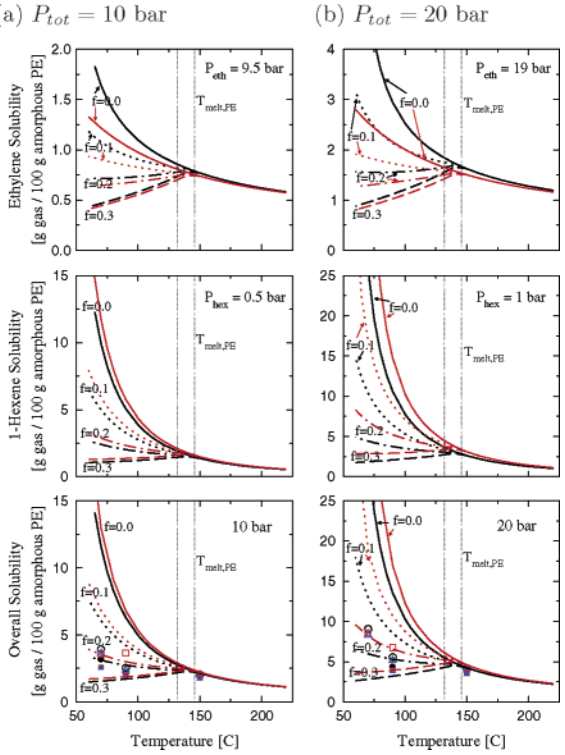

Figure 11. Elastic effect on gas solubilities in linear C_{1000} in ternary mixtures of ethylene/1-hexene/linear C_{1000} at total pressures of 10 and 20 bar. Unless otherwise specified, the ternary mixture gas-phase composition is 95 mol % ethylene/5 mol % 1-hexene (P_{eth} = 9.5 bar and P_{hex} = 0.5 bar at P_{tot} = 10 bar; P_{eth} = 19 bar and P_{hex} = 1 bar at P_{tot} = 20 bar). The black curves (—, ···, -·-, - -) are ternary mixture PC−SAFT predictions corrected with elastic contraints (f) as indicated in the graphs. The PC−SAFT result with no elastic effect, f = 0.0, is the prediction fitted to simulation results. The red curves (—, ···, -·-, - -) are binary monomer/C_{1000} PC−SAFT predictions corrected with elastic constraints (f) as indicated in the graphs, ●, ■, and ▲ are experimental overall solubility results in ethylene-1-hexene copolymers of 100, 96.12, and 95.25 mol % ethylene incorporated in the polyolefin (PE000, PE388, and PE475 from Table 6), respectively from Novak et al.[22] The gas-phase composition for the experimental results is 95.7 mol % ethylene/4.3 mol % 1-hexene. ○, □, and △ are overall solubility results in ethylene-1-hexene copolymers of 100, 96.12, and 95.25 mol % ethylene incorporated in the polyolefin (PE000, PE388, and PE475 from Table 6), respectively from Novak et al.[22] as expected from summing the binary monomer/polymer mixture results.

1-hexene increases the solubility of ethylene in the polymer, thereby enhancing the reaction rate. Our predictions indicate that ethylene solubility is indeed enhanced by as much as 7−10% due to the presence of 1-hexene at typical polymerization reactor temperatures of 70−100 °C, with f = 0.2 for elastic constraints. This solubility effect alone would account for about a 7−10% increase in the apparent polymerization rate as a result of adding 1-hexene to the gas phase. While this solubility enhancement effect does not completely explain the enhancement in polymerization rate, it clearly substantiates one of the factors contributing to the observed polymerization rate enhancement. It is also noted here that, in some situations, enhanced rates of diffusion may also be an important contributing factor since the ternary mixture swells much more than the binary ethylene/polyethylene mixture.

6. Conclusions

It has been shown in this work that the recently proposed osmotic-ensemble hyperparallel tempering molecular simulation technique[1] provides an effective method for parametrization of an equation of state appropriate for polymeric systems. Specifically, the method has been used to parametrize the PC−SAFT equation of state without the use of a priori experimental results. The resulting parametrization is capable of describing simulation results for properties other than those for which the fitting procedure is performed. For ethylene/polyethylene mixtures, the fitted PC−SAFT model agrees well with solubility and amorphous polymer phase density simulation results. For 1-hexene/polyethylene and ternary ethylene/1-hexene/polyethylene mixtures, the fitted PC−SAFT model agrees well with simulation results at higher temperatures but is seen to overpredict solubilities at lower temperatures (below 100 °C); the equation of state exhibits a tendency to overpredict polymer swelling in these cases.

From simulations of different ethylene and 1-hexene copolymers, it has been observed that short-chain branching has no effect on monomer solubilities for typical LLDPE conditions. This confirms results of earlier calculations,[1] and it is now verified by experimental results.[22]

Upon comparing predictions for binary and ternary mixtures, it is observed that the inclusion of 1-hexene gas enhances the ethylene solubility in polyethylene. The inclusion of ethylene gas, however, decreases the 1-hexene solubility, leading to an overall decrease in gas solubility with respect to that predicted by summing results for the two binary systems. Therefore, while chain architecture (short-chain branching) does not enhance solubility, the presence of 1-hexene in the gas phase increases the solubility of ethylene in the polymer. We propose that this ethylene solubility enhancement contributes to the polymerization reaction rate increase that is observed when 1-hexene is used as a comonomer.[15,16,18] Experimental data validate our prediction that the overall solubility slightly decreases in the ternary mixture. These data, however, hide the fact—revealed by simulations—that ethylene solubility is enhanced.

Elastic constraints are seen to play an important role for temperatures below the polymer melting temperature. As shown in this work, the simulation fitted PC−SAFT model accurately predicts solubilities for temperatures above the melting point. Below the melting point, a modified PC−SAFT model is also able to describe experimental data. Our findings suggest that the elastic constraint parameter introduced to quantify the effect of semicrystallinity on solubility is not strongly dependent on the particular solvents dissolved in the given nascent polyethylene. For this approach to be fully predictive, a priori knowledge is required for the fraction of "elastically affected" chains. It is believed that this information could be obtained by following the experimental approach of studying "constrained interphases" in semicrystalline polyethylene.[12−14]

Acknowledgment. The authors are grateful to Walter Chapman and Auleen Ghosh at Rice University for supplying and supporting a code for PC−SAFT equation of state. Financial support from the U.S. Department of Energy (DE-FG02-99ER14961) and the industrial sponsors of the University of Wisconsin

Polymerization Reaction Engineering Laboratory is also gratefully acknowledged.

Supporting Information Available: Text giving derivations for eqs 17 and 18 and elastic effects on the amorphous polymer phase pressure and chemical potentials. This material is available free of charge via the Internet at http://pubs.acs.org.

References and Notes

(1) Banaszak, B. J.; Faller, R.; de Pablo, J. J. *J. Chem. Phys.* **2004**, *120*, 11304−11315.
(2) Gross, J.; Sadowski, G. *Ind. Eng. Chem. Res.* **2001**, *40*, 1244−1260.
(3) Gross, J.; Sadowski, G. *Ind. Eng. Chem. Res.* **2002**, *41*, 1084−1093.
(4) Tumakaka, F.; Gross, J.; Sadowski, G. *Fluid Phase Equilib.* **2002**, 194−197, 541−551.
(5) Chapmann, W. G.; Gubbins, K. E.; Jackson, G.; Radosz, M. *Ind. Eng. Chem. Res.* **1990**, *29*, 1709−1721.
(6) Huang, S. H.; Radosz, M. *Ind. Eng. Chem. Res.* **1990**, *29*, 2284−2294.
(7) Huang, S. H.; Radosz, M. *Ind. Eng. Chem. Res.* **1991**, *30*, 1994−2005.
(8) Chapmann, W. G.; Gubbins, K. E.; Jackson, G.; Radosz, M. *Fluid Phase Equilib.* **1989**, *52*, 31−38.
(9) Michaels, A. S.; Hausslein, R. W. *J. Polym. Sci. C* **1965**, *61*, 61−86.
(10) Doong, S. J.; Ho, W. S. W. *Ind. Eng. Chem. Res.* **1991**, *30*, 1351−1361.
(11) Hedenqvist, M.; Gedde, U. W. *Prog. Polym. Sci.* **1996**, *21*, 299−333.
(12) Kitamaru, R.; Horii, F.; Murayama, K. *Macromolecules* **1986**, *19*, 636−643.
(13) Mandelkern, L.; McLaughlin, K. W.; Alamo, R. G. *Macromolecules* **1992**, *25*, 1440−1444.
(14) Mutter, R.; Stille, W.; Strobl, G. *J. Polym. Sci., Part B:* **1993**, *31*, 99−105.
(15) Ray, W. H. In *Transition Metal Catalyzed Polymerizations: Ziegler−Natta and Metathesis Polymerizations*; Quirk, R. P., Ed.; Cambridge University Press: New York, 1989.
(16) Han-Adebekun, G. C.; Ray, W. H. *J. Appl. Polym. Sci.* **1997**, *65*, 1037−1052.
(17) Koivumäki, J.; Seppälä, J. V. *Macromolecules* **1993**, *26*, 5535−5538.
(18) Kumkaew, P.; Wu, L.; Praserthdam, P.; Wanke, S. E. *Polymer* **2003**, *44*, 4791−4803.
(19) dos Santos, J. H. Z.; Uozumi, T.; Teranishi, T.; Sano, T.; Soga, K. *Polymer* **2001**, *42*, 4517−4525.
(20) Nath, S. K.; de Pablo, J. J. *J. Phys. Chem. B* **1999**, *103*, 3539−3544.
(21) Nath, S. K.; Banaszak, B. J.; de Pablo, J. J. *Macromolecules* **2001**, *34*, 7841−7848.
(22) Novak, A.; Bobak, M.; Kosek, J.; Banaszak, B. J.; Lo, D.; Widya, T.; Ray, W. H.; de Pablo, J. J. Manuscript in preparation, 2004.
(23) Nath, S. K.; Escobedo, F. A.; de Pablo, J. J. *J. Chem. Phys.* **1998**, *108*, 9905−9911.
(24) Nath, S. K.; de Pablo, J. *J. Mol. Phys.* **2000**, *98*, 231−238.
(25) Nath, S. K.; Banaszak, B. J.; de Pablo, J. J *J. Chem. Phys.* **2001**, *114*, 3612−3616.
(26) Jorgensen, W. L.; Madura, J. D.; Swensen, C. J. *J. Am. Chem. Soc.* **1984**, *106*, 6638−6646.
(27) Nath, S. K.; Escobedo, F. A.; de Pablo, J. J.; Patramai, I. *Ind. Eng. Chem. Res.* **1998**, *37*, 3195−3202.
(28) Frenkel, D.; Smit, B. *Understanding Molecular Simulation: From Algorithms to Applications*; Academic Press: New York, 1996; pp 31−33, 157−163, 291−300, 316−332.
(29) Allen, M. P.; Tildesley, D. J. *Computer Simulation of Liquids*; Oxford University Press: New York, 1987; pp 64−65.
(30) Duane, S.; Kennedy, A. D.; Pendleton, B. J.; Roweth, D. *Phys. Lett. B* **1987**, *195*, 216−222.
(31) Nath, S. K.; de Pablo, J. J.; DeBellis, A. D. *J. Am. Chem. Soc.* **1999**, *121*, 4252−4261.
(32) Laso, M.; de Pablo, J. J.; Suter, U. W. *J. Chem. Phys.* **1992**, *97*, 2817−2819.
(33) Escobedo, F. A.; de Pablo, J. J. *J. Chem. Phys.* **1996**, *105*, 4391−4394.
(34) Siepmann, J. I.; Frenkel, D. *Mol. Phys.* **1992**, *75*, 59−70.
(35) Chen, Z.; Escobedo, F. A. *J. Chem. Phys.* **2000**, *113*, 11382−11392.
(36) Faller, R.; de Pablo, J. J. *J. Chem. Phys.* **2002**, *116*, 55−59.
(37) Faller, R.; de Pablo, J. J. *J. Chem. Phys.* **2003**, *119*, 7605.
(38) Yan, Q.; de Pablo, J. J. *J. Chem. Phys.* **1999**, *111*, 9509−9516.
(39) Yan, Q.; de Pablo, J. J. *J. Chem. Phys.* **2000**, *113*, 1276−1282.
(40) Hansmann, U. H. E. *Chem. Phys. Lett.* **1997**, *281*, 140−150.
(41) Rosenbluth, M. N.; Rosenbluth, A. W. *J. Chem. Phys.* **1955**, *23*, 356−359.
(42) Flory, P. J.; Rehner, J. *J. Chem. Phys.* **1943**, *11*, 521−526.
(43) Rogers, C. E.; Stannett, V.; Szwarc, M. *J. Phys. Chem.* **1959**, *63*, 1406−1413.
(44) Yoon, J. S.; Yoo, H. S.; Kang, K. S. *Eur. Polym. J.* **1996**, *32*, 1333−1336.
(45) Moore, S. J.; Wanke, S. E. *Chem. Eng. Sci.* **2001**, *56*, 4121−4129.
(46) Dee, G. T.; Ougizawa, T.; Walsh, D. J. *Polymer* **1992**, *33*, 3462−3469.
(47) Maloney, D. P.; Prausnitz, J. M. *AIChE J.* **1976**, *22*, 74−82.

MA0491107